Smart Mater. Struct. **17** (2008) 055007 (13pp) doi:10.1088/0964-1726/17/5/055007

Smart constrained layer damping of functionally graded shells using vertically/obliquely reinforced 1–3 piezocomposite under a thermal environment

M C Ray and R C Batra

Department of Engineering Science and Mechanics, MC 0219, Virginia Polytechnic Institute and State University, Blacksburg, VA 24061, USA

Received 19 January 2008, in final form 23 June 2008
Published 1 August 2008
Online at stacks.iop.org/SMS/17/055007

Abstract

We analyze active constrained layer damping (ACLD) of functionally graded (FG) shells under a thermal environment using vertically and obliquely reinforced 1–3 piezocomposites (PZCs) and investigate the performance of PZCs as materials for the constraining layer of the ACLD treatment. The shell's deformations are analyzed by using a modified first-order shear deformation theory and the finite element method. A temperature gradient is applied across the thickness of the shell. Both in-plane and out-of-plane actuations of the constraining layer of the ACLD treatment have been utilized. Particular emphasis has been placed on ascertaining the performance of patches when the orientation angle of the piezoelectric fibers in the constraining layer is varied in two mutually orthogonal vertical planes. It is found that the vertical actuation dominates over the in-plane actuation, and distributed actuators made of vertically and obliquely reinforced 1–3 PZCs have great potential for controlling the performance of FG shells under a thermal environment.

1. Introduction

In an endeavor to develop super heat resistant materials, Koizumi [1] proposed the concept of functionally graded materials (FGMs) which exhibit smooth variation of material properties in one direction. The laminated composite structures can be tailored to have high stiffness to weight and high strength to weight ratios, and improved thermal and transport properties. However, the sharp change in properties at the interface between two adjacent layers may induce large interlaminar shear stresses which may cause delamination. Such detrimental effects can be circumvented if material properties vary smoothly in the thickness direction. For example, Aboudi *et al* [2] have analyzed a thermomechanical problem for FG structures with material properties varying continuously in two directions and demonstrated that the delamination could be avoided by tailoring the microstructures of composite plies. The FGMs have been viewed as a new class of advanced materials for designing structures. Several investigators (e.g. see [3–7]) have provided exact solutions to initial-boundary-value problems for structures comprised of FGMs, and have studied their dynamic and buckling responses.

A lightweight high performance flexible structure is desired to have self-controlling and self-monitoring capabilities which can be attained by using distributed piezoelectric (PZT) actuators and sensors either mounted on or embedded in the structure [8–12]; such structures are customarily known as 'smart structures'. Considerable interest has also been focused on investigating the performance of FG plates and shells having PZT actuators [13–21]. The control authority of existing monolithic PZT materials is very low because of the very small magnitude of their stress/strain coefficients. Research on the efficient use of these PZTs has led to the development of the active constrained layer damping (ACLD) treatment [22] which consists of a layer of a viscoelastic material constrained between a host structure and an active constraining PZT layer. When the constraining layer is not subjected to any control voltage and the host structure vibrates, the constrain-

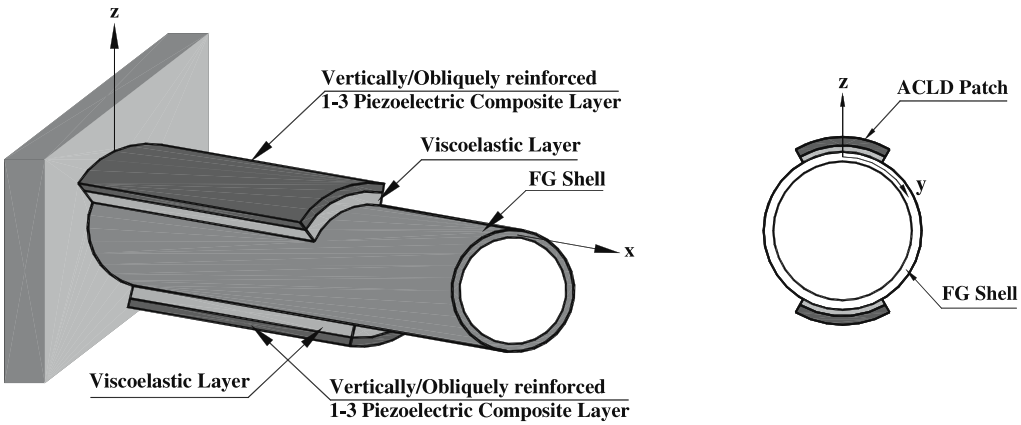

Figure 1. Schematics of an FG shell integrated with patches of ACLD treatment comprised of a 1–3 PZC constraining layer.

ing layer behaves passively and restrains the constrained viscoelastic layer to undergo transverse shear deformations. This set-up is called passive constrained layer damping. However, if deformations of the constraining layer are appropriately controlled to enhance the transverse shear deformations of the constrained viscoelastic layer, the damping of the structure is improved and the structure is said to undergo active constrained layer damping. Since the control effort necessary to increase the transverse shear deformations of the constrained viscoelastic layer is compatible with the low control authority of monolithic PZTs, PZTs are often used as the constraining layer material. The ACLD treatment has been extensively used to efficiently and reliably control vibrations of flexible structures [23–28].

Piezocomposites (PZCs), comprised of epoxy matrix reinforced with PZT fibers, are often used as distributed actuators and sensors. These PZCs provide a wide range of effective material properties not offered by monolithic PZTs, and are characterized by good conformability and strength. Of several PZCs, the one often studied is the vertically reinforced 1–3 PZC [29, 30] which is commercially available[1] as a lamina. This is being effectively used as an underwater transducer, a high frequency ultrasonic transducer [29, 30] and in medical imaging applications. The PZT fibers in a 1–3 PZC are poled along their length, and the top and the bottom surfaces of the lamina are electroded. A micromechanical analysis [29] has revealed that the magnitude of the effective piezoelectric coefficient e_{33} of this PZC is much larger than that of the effective coefficient e_{31}. Note that magnitudes of e_{33} and e_{31} signify, respectively, the induced actuating normal (along the fiber direction) and shear stresses due to a unit electric field applied across the thickness of the PZT lamina Therefore, if a voltage is applied across the surface electrodes of a 1–3 PZC lamina, the transverse normal stress (σ_z) induced in the thickness direction will be much larger than the induced in-plane normal stress (σ_x). This can be exploited to control flexural vibrations of the host structure. Hence, considerable efforts have been made to enhance the value of e_{33} in a 1–3 PZC for causing electromechanical transduction. These PZCs also have improved mechanical performance, electromechanical coupling characteristics and acoustic impedance matching over existing monolithic PZTs [29]. However, very little attention has been paid to using these commercially available 1–3 PZCs as distributed actuators in smart structures. Recently, Ray and Prodhan [31, 32] and Ray and Batra [33] have shown that the vertical actuation of 1–3 PZCs causes significant damping of smart laminated composite beams and plates. Also, instead of having the reinforcing PZT fibers vertical, one can make them oblique in the vertical plane (see footnote 1) and take advantage of the actuation caused by both e_{33} and e_{31}. Batra and Geng [34] have analyzed 3D deformations of a laminated plate with ACLD layers bonded to its top surface. The PZT constraining layers were poled at an angle to the vertical direction so that both transverse and normal strains in the PZT layers induced transverse shear deformation of the constrained viscoelastic layer whose material response was simulated by a hereditary type integral with the shear modulus expressed in terms of a Prony series. They assumed that the viscoelastic layer was made of an FG material whose relaxation time varied continuously through the thickness.

An FG circular cylindrical shell is an important structural element. It seems that the performance of 1–3 PZCs for active vibration control of FG shells under thermal environment has not been studied. Here, we study by the finite element method (FEM) three-dimensional (3D) deformations of an FG shell integrated with patches of ACLD treatment and subjected to a temperature gradient across its thickness. We also delineate the effect of the PZT fiber orientation in two mutually orthogonal vertical planes on the performance of ACLD patches.

2. Problem description and formulation

Figure 1 illustrates a circular cylindrical FG shell whose outer surface is integrated with rectangular ACLD patches with the constraining layer made of either vertically or obliquely reinforced 1–3 PZCs; details of a 1–3 PZC are shown in figure 2. Even though PZT fibers in figure 2 have rectangular cross section, the problem formulation and analysis is applicable to all prismatic fibers of any cross section so long as their volume fraction is kept constant. For an obliquely

[1] Piezocomposites, Materials Systems Inc., 543 Great Road, Littleton, MA 01460, USA.

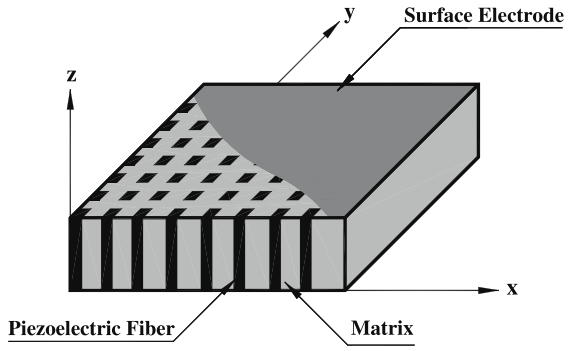

(a) **Lamina of a vertically reinforced 1-3 PZC**

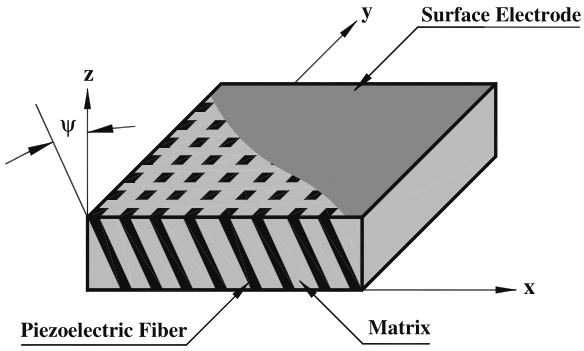

(b) **PZT fibers are coplanar with the vertical xz - plane**

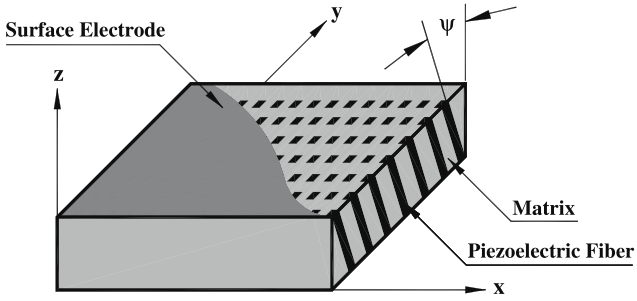

(c) **Piezoelectric fibers are coplanar with vertical yz - plane**

Figure 2. Schematics of a lamina of a vertically and obliquely reinforced 1–3 PZC.

reinforced 1–3 PZC, the PZT fibers are coplanar with either the vertical xz or the vertical yz plane making an angle ψ with the z axis. Thicknesses of the substrate FG shell, the PZC layer and the viscoelastic layer are denoted by h, $h_{\rm p}$ and $h_{\rm v}$, respectively, while the average radius of the shell is denoted by R. The mid-plane of the shell is taken as the reference plane and the origin of the reference curvilinear coordinate system (xyz) is located on this reference plane such that curves $x = 0$ and a represent, respectively, the fixed and the free ends of the shell. Temperatures of the ceramic-rich and the metal-rich surfaces of the FG shell are denoted by $T_{\rm c}$ and $T_{\rm m}$, respectively. It is assumed that the FG shells are stress-free at the ambient temperature T_0, and temperature changes in the ACLD patches are neglected. It is also assumed that the temperature in the shell varies only in the thickness or the z direction.

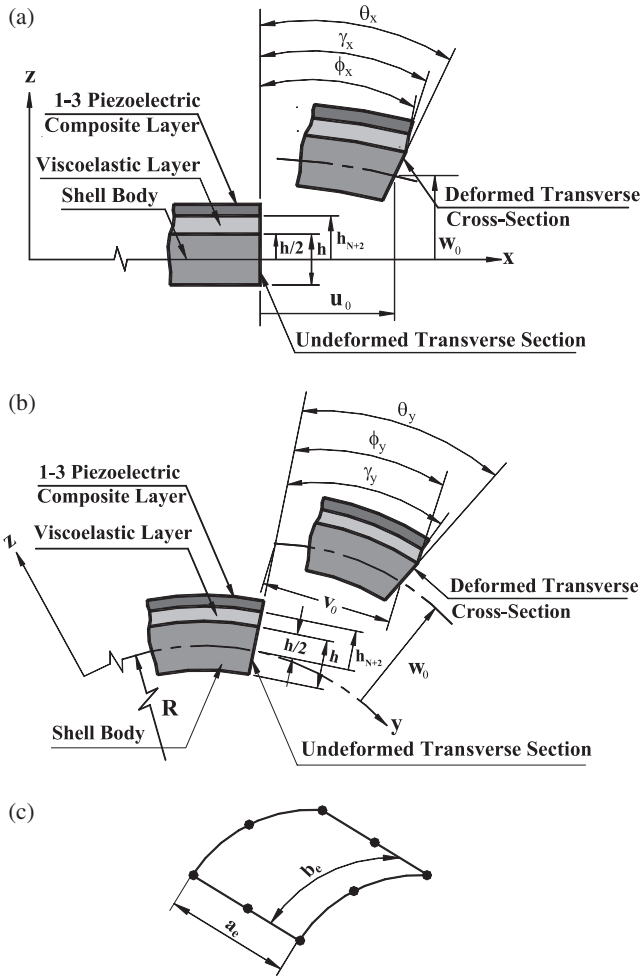

Figure 3. Kinematics of deformations of transverse cross sections which are parallel to (a) the xz and (b) the yz planes, and (c) a typical eight-node finite element.

The shell is assumed to be thin and consequently the first-order shear deformation theory (FSDT) modified to account for transverse normal strains is used to analyze deformations of the shell, the constrained layer and the ACLD patches. Figure 3 illustrates kinematic variables used in the FSDT; u_0 and v_0 represent the generalized translational displacement of a point (x, y) of the reference plane $(z = 0)$ along the x and y directions, respectively; θ_x, ϕ_x and γ_x denote generalized rotations in the xz plane of normals to mid-planes of the substrate shell, the viscoelastic layer and the PZC layer, respectively; θ_y, ϕ_y and γ_y represent rotations of these normal vectors in the yz plane. Thus axial displacements u and v along the x and y directions, respectively, of a point of the structure can be expressed as

$$u(x, y, z, t) = u_0(x, y, t) + (z - \langle z - h/2\rangle)\theta_x(x, y, t) + (\langle z - h/2\rangle - \langle z - h_{N+2}\rangle)\phi_x(x, y, t) + \langle z - h_{N+2}\rangle\gamma_x(x, y, t) \quad (1)$$

$$v(x, y, z, t) = v_0(x, y, t) + (z - \langle z - h/2\rangle)\theta_y(x, y, t) + (\langle z - h/2\rangle - \langle z - h_{N+2}\rangle)\phi_y(x, y, t) + \langle z - h_{N+2}\rangle\gamma_y(x, y, t), \quad (2)$$

where a function within the bracket $\langle\,\rangle$ represents an appropriate singularity function for satisfying continuity conditions at an interface between any two adjoining continua.

As mentioned in section 1 and in [31, 32], in order to use the 1–3 PZC as a distributed actuator, transverse actuation induced by the PZC must be utilized. Hence, the transverse normal strain in the overall shell must be considered. Batra *et al* [35, 36] have developed a variable order shear and normal deformable theory for anisotropic piezoelectric plates that satisfies exactly the normal and tangential tractions prescribed on the top and the bottom surfaces of a plate. Here, however, for simplicity we assume the transverse displacement w at a point in the FG substrate shell, the viscoelastic layer and the PZC layer to vary affinely across their thicknesses. That is,

$$\begin{aligned} w(x,y,z,t) &= w_0(x,y,t) + (z - \langle z - h/2\rangle)\theta_z(x,y,t) \\ &\quad + (\langle z - h/2\rangle - \langle z - h_{N+2}\rangle)\phi_z(x,y,t) \\ &\quad + \langle z - h_{N+2}\rangle\,\gamma_z(x,y,t), \end{aligned} \tag{3}$$

where w_0 is the transverse displacement of a point on the reference plane; θ_z, ϕ_z and γ_z are the generalized displacements representing gradients, with respect to the thickness coordinate z, of the transverse displacement in the shell, the viscoelastic layer and the PZC layer, respectively. For brevity, the generalized displacement variables are grouped as

$$\begin{aligned} \{d_t\} &= [\,u_0 \quad v_0 \quad w_0\,]^{\mathrm{T}} \qquad \text{and} \\ \{d_r\} &= [\,\theta_x \quad \theta_y \quad \theta_z \quad \phi_x \quad \phi_y \quad \phi_z \quad \gamma_x \quad \gamma_y \quad \gamma_z\,]^{\mathrm{T}}. \end{aligned} \tag{4}$$

In order to employ the reduced integration rule for computing element stiffness matrices corresponding to transverse shear deformations, the state of strain at a point is divided into the following two strain vectors:

$$\begin{aligned} \{\in_b\} &= [\,\in_x \quad \in_y \quad \in_{xy} \quad \in_z]^{\mathrm{T}} \\ \text{and} \qquad \{\in_s\} &= [\,\in_{xz} \quad \in_{yz}\,]^{\mathrm{T}} \end{aligned} \tag{5}$$

in which $\in_x$, $\in_y$, $\in_z$ are the normal strains along the x, y and z directions, respectively, $\in_{xy}$ is the in-plane shear strain, and $\in_{xz}$, $\in_{yz}$ are the transverse shear strains. Using displacement fields (1)–(3), the linear strain–displacement relations and equation (5), vectors $\{\in_b\}_{\mathrm{FG}}$, $\{\in_b\}_{\mathrm{v}}$ and $\{\in_b\}_{\mathrm{p}}$ defining the in-plane and the transverse normal strains at a point in the shell, the viscoelastic layer and the active constraining layer, respectively, can be expressed as

$$\begin{aligned} \{\in_b\}_{\mathrm{FG}} &= \{\in_{bt}\} + [Z_1]\{\in_{br}\}, \\ \{\in_b\}_{\mathrm{v}} &= \{\in_{bt}\} + [Z_2]\{\in_{br}\} \\ \text{and} \qquad \{\in_b\}_{\mathrm{p}} &= \{\in_{bt}\} + [Z_3]\{\in_{br}\}. \end{aligned} \tag{6}$$

Similarly, vectors $\{\in_s\}_{\mathrm{FG}}$, $\{\in_s\}_{\mathrm{v}}$ and $\{\in_s\}_{\mathrm{p}}$ defining the transverse shear strains at a point in the shell, the viscoelastic layer and the active constraining layer, respectively, can be expressed as

$$\begin{aligned} \{\in_s\}_{\mathrm{FG}} &= \{\in_{st}\} + [Z_4]\{\in_{sr}\}, \\ \{\in_s\}_{\mathrm{v}} &= \{\in_{st}\} + [Z_5]\{\in_{sr}\} \\ \text{and} \qquad \{\in_s\}_{\mathrm{p}} &= \{\in_{st}\} + [Z_6]\{\in_{sr}\} \end{aligned} \tag{7}$$

where matrices are defined in the appendix, and the generalized strain vectors are defined below:

$$\begin{aligned} \{\in_{bt}\} &= [\,\tfrac{\partial u_0}{\partial x} \quad \tfrac{\partial v_0}{\partial y} + \tfrac{w}{R} \quad \tfrac{\partial u_0}{\partial y} + \tfrac{\partial v_0}{\partial x} \quad 0\,]^{\mathrm{T}}, \\ \{\in_{st}\} &= [\,\tfrac{\partial w_0}{\partial x} \quad \tfrac{\partial w_0}{\partial y} - \tfrac{v_0}{R}\,]^{\mathrm{T}}, \\ \{\in_{br}\} &= [\,\tfrac{\partial \theta_x}{\partial x} \quad \tfrac{\partial \theta_y}{\partial y} \quad \tfrac{\partial \theta_x}{\partial y} + \tfrac{\partial \theta_y}{\partial x} \quad \theta_z \quad \tfrac{\partial \phi_x}{\partial x} \quad \tfrac{\partial \phi_y}{\partial y} \\ &\qquad \tfrac{\partial \phi_x}{\partial y} + \tfrac{\partial \phi_y}{\partial x} \quad \phi_z \quad \tfrac{\partial \gamma_x}{\partial x} \quad \tfrac{\partial \gamma_y}{\partial y} \quad \tfrac{\partial \gamma_x}{\partial y} + \tfrac{\partial \gamma_y}{\partial x} \quad \gamma_z\,]^{\mathrm{T}} \\ \text{and} \quad \{\in_{sr}\} &= [\,\theta_x \quad \theta_y \quad \phi_x \quad \phi_y \quad \gamma_x \quad \gamma_y \\ &\qquad \tfrac{\partial \theta_z}{\partial x} \quad \tfrac{\partial \theta_z}{\partial y} \quad \tfrac{\partial \phi_z}{\partial x} \quad \tfrac{\partial \phi_z}{\partial y} \quad \tfrac{\partial \gamma_z}{\partial x} \quad \tfrac{\partial \gamma_z}{\partial y}\,]. \end{aligned} \tag{8}$$

Similar to the strain vectors given by equation (5), stresses at a point in the structure are grouped as

$$\begin{aligned} \{\sigma_b\} &= [\,\sigma_x \quad \sigma_y \quad \sigma_{xy} \quad \sigma_z\,]^{\mathrm{T}} \\ \text{and} \qquad \sigma_s &= [\,\sigma_{xz} \quad \sigma_{yx}\,]^{\mathrm{T}}, \end{aligned} \tag{9}$$

where σ_x, σ_y and σ_z are normal stresses along the x, y and z directions, respectively; σ_{xy} is the in-plane shear stress; σ_{xz} and σ_{yz} are the transverse shear stresses.

The FG substrate shell is presumed to be comprised of two homogeneous materials, namely, a ceramic and a metal. We assume that the FGM is isotropic and linear elastic, volume fractions of constituents vary only in the thickness direction according to a power law, and the effective material properties are given by the rule of mixtures. Young's modulus (E_{FG}), the mass density (ρ_{FG}), the coefficient of thermal expansion (α_{FG}) and the thermal conductivity (κ_{FG}) at a point can be expressed as

$$\begin{aligned} E_{\mathrm{FG}}(z) &= (E_{\mathrm{c}} - E_{\mathrm{m}})\left\{\frac{1}{2} + (-1)^k\frac{z}{h}\right\}^n + E_{\mathrm{m}}, \\ \rho_{\mathrm{FG}}(z) &= (\rho_{\mathrm{c}} - \rho_{\mathrm{m}})\left\{\frac{1}{2} + (-1)^k\frac{z}{h}\right\}^n + \rho_{\mathrm{m}}, \\ \alpha_{\mathrm{FG}}(z) &= (\alpha_{\mathrm{c}} - \alpha_{\mathrm{m}})\left\{\frac{1}{2} + (-1)^k\frac{z}{h}\right\}^n + \alpha_{\mathrm{m}} \\ \text{and} \qquad \kappa_{\mathrm{FG}}(z) &= (\kappa_{\mathrm{c}} - \kappa_{\mathrm{m}})\left\{\frac{1}{2} + (-1)^k\frac{z}{h}\right\}^n + \kappa_{\mathrm{m}}. \end{aligned} \tag{10}$$

Here subscripts c and m denote, respectively, quantities for the ceramic and the metal, respectively, n is the power law exponent and k is a positive integer. When k is even, the inner surface of the FG shell is metallic (softest) while the outer surface of the shell is ceramic (stiffest) and the reverse holds when k is odd. Thus the outer surface of the FG shell can be modeled either as the softest or as the stiffest surface according to whether k equals 1 or 2, respectively. Poisson's ratio ν of the FGM is considered to be a constant [7]. Constitutive relations for the material of the substrate FG shell can be expressed as

$$\begin{aligned} \{\sigma_b\}_{\mathrm{FG}} &= [C_b]_{\mathrm{FG}}(\{\in_b\}_{\mathrm{FG}} - \{\bar{\alpha}\}\Delta T) \\ \text{and} \qquad \{\sigma_s\}_{\mathrm{FG}} &= [C_s]_{\mathrm{FG}}\{\in_b\}_{\mathrm{FG}} \end{aligned} \tag{11}$$

in which $\Delta T = T(z) - T_0$. The elastic coefficient matrices $[C_b]_{\mathrm{FG}}$ and $[C_s]_{\mathrm{FG}}$, and the vector $\{\bar{\alpha}\}$ of thermal expansion

coefficients are given by

$$
\begin{aligned}
[C_b]_{\mathrm{FG}} &= [C_b]_{\mathrm{m}}\left[1+\left(\frac{E_{\mathrm{c}}}{E_{\mathrm{m}}}-1\right)\left\{\frac{1}{2}+(-1)^k\frac{z}{h}\right\}^n\right],\\
[C_s]_{\mathrm{FG}} &= [C_s]_{\mathrm{m}}\left[1+\left(\frac{E_{\mathrm{c}}}{E_{\mathrm{m}}}-1\right)\left\{\frac{1}{2}+(-1)^k\frac{z}{h}\right\}^n\right],\\
[C_b]_{\mathrm{m}} &= \frac{E_{\mathrm{m}}}{(1+\nu)(1-2\nu)}\\
&\quad\times\begin{bmatrix}(1-\nu) & \nu & 0 & \nu\\ \nu & (1-\nu) & 0 & \nu\\ 0 & 0 & (1-2\nu)/2 & 0\\ \nu & \nu & 0 & (1-\nu)\end{bmatrix},\\
[C_s]_{\mathrm{m}} &= \frac{E_{\mathrm{m}}}{2(1+\nu)}\begin{bmatrix}1 & 0\\ 0 & 1\end{bmatrix}\\
\text{and}\qquad \{\bar{\alpha}\} &= [\,\alpha(z)\quad \alpha(z)\quad 0\quad \alpha(z)\,]^{\mathrm{T}}.
\end{aligned}
\tag{12}
$$

The temperature distribution $T(z)$ across the thickness of the FG substrate shell determined by solving the following 1D steady state heat conduction equation [5]:

$$
-\frac{\mathrm{d}}{\mathrm{d}z}\left\{\kappa(z)\frac{\mathrm{d}T(z)}{\mathrm{d}z}\right\}=0 \tag{13}
$$

is given by [5]

$$
T(z)=T_{\mathrm{c}}+\frac{T_{\mathrm{m}}-T_{\mathrm{c}}}{\int_{-h/2}^{h/2}\frac{1}{\kappa(z)}\,\mathrm{d}z}\int_{-h/2}^{z}\frac{1}{\kappa(z)}\,\mathrm{d}z. \tag{14}
$$

The constrained layer of the ACLD treatment patch is assumed to be linear viscoelastic, homogeneous and isotropic, and its material response is modeled by using the complex modulus. That is, the shear modulus G_{v}, Young's modulus E_{v} and the constitutive relation of the viscoelastic material are given by [22, 23]

$$
\begin{aligned}
&G_{\mathrm{v}}=G'(1+\mathrm{i}\eta),\qquad E_{\mathrm{v}}=2G_{\mathrm{v}}(1+\nu_{\mathrm{v}}),\\
&\{\sigma_b\}_{\mathrm{v}}=[C_b]_{\mathrm{v}}\{\in_b\}_{\mathrm{v}}\qquad\text{and}\qquad \{\sigma_s\}_{\mathrm{v}}=[C_s]_{\mathrm{v}}\{\in_b\}_{\mathrm{v}}
\end{aligned}
\tag{15}
$$

where G' is the storage modulus, ν_{v} is Poisson's ratio and η is the loss factor at a particular operating temperature and frequency. Note that using E_{v} and ν_{v} in place of E_{m} and ν, respectively, in expressions (12) for $[C_b]_{\mathrm{m}}$ and $[C_s]_{\mathrm{m}}$, $[C_b]_{\mathrm{v}}$ and $[C_s]_{\mathrm{v}}$ can be determined. We neglect the dependence of elastic moduli upon the temperature, and heat generated in the layer due to viscous dissipation.

Following Smith and Auld [29], constitutive relations for the vertically reinforced ($\psi=0°$) 1–3 PZC are given by

$$
\begin{aligned}
\{\sigma\}_{\mathrm{p}} &= [C]_{\mathrm{p}}\{\in\}_{\mathrm{p}}-[e]\{E\}\\
\text{and}\qquad \{D\} &= [e]^{\mathrm{T}}\{\in\}_{\mathrm{p}}+[\varepsilon]\{E\}
\end{aligned}
\tag{16}
$$

in which $[C]_{\mathrm{p}}$, $[e]$ and $[\varepsilon]$ are the effective elastic, piezoelectric and dielectric constant matrices, respectively. The explicit form of $[C]_{\mathrm{p}}$ resembles that of an orthotropic material while the explicit forms of $[e]$ and $[\varepsilon]$ are given by

$$
\begin{aligned}
[e]^{\mathrm{T}} &= \begin{bmatrix}0 & 0 & 0 & 0 & e_{15} & 0\\ 0 & 0 & 0 & e_{24} & 0 & 0\\ e_{31} & e_{32} & e_{33} & 0 & 0 & 0\end{bmatrix}\\
\text{and}\qquad [\varepsilon] &= \begin{bmatrix}\varepsilon_{11} & 0 & 0\\ 0 & \varepsilon_{22} & 0\\ 0 & 0 & \varepsilon_{33}\end{bmatrix}.
\end{aligned}
\tag{17}
$$

In equation (16), expressions for the stress $\{\sigma\}$ and the strain $\{\in\}$ vectors are not similar to those given in equations (5) and (9) but are given by

$$
\begin{aligned}
\{\sigma\} &= [\,\sigma_x\quad \sigma_y\quad \sigma_z\quad \sigma_{yz}\quad \sigma_{xz}\quad \sigma_{xy}\,]^{\mathrm{T}}\\
\text{and}\qquad \{\in\} &= [\,\in_x\quad \in_y\quad \in_z\quad \in_{yz}\quad \in_{xz}\quad \in_{xy}\,]^{\mathrm{T}}
\end{aligned}
\tag{18}
$$

while the electric field $\{E\}$ and the electric displacement $\{D\}$ vectors are given by

$$
\begin{aligned}
\{E\} &= [\,E_x\quad E_y\quad E_z]^{\mathrm{T}}\\
\text{and}\qquad \{D\} &= [\,D_x\quad D_y\quad D_z]^{\mathrm{T}}.
\end{aligned}
\tag{19}
$$

Here E_x, E_y and E_z are electric fields along the x, y and z directions, respectively, and D_x, D_y and D_z are the corresponding electric displacements. When fibers of the 1–3 PZC are coplanar with the vertical xz or yz plane but are oriented at an angle ψ with respect to the z axis as shown in figure 2, constitutive relations for the PZC with respect to the reference coordinate system (xyz) are derived by employing the appropriate transformation law:

$$
\begin{aligned}
&\{\sigma\}_{\mathrm{p}}=[\bar{C}]_{\mathrm{p}}\{\in\}_{\mathrm{p}}-[\bar{e}]\{E\}\qquad\text{and}\\
&\{D\}=[\bar{e}]^{\mathrm{T}}\{\in\}_{\mathrm{p}}+[\bar{\varepsilon}]\{E\},
\end{aligned}
\tag{20}
$$

where

$$
\begin{aligned}
&[\bar{C}]_{\mathrm{p}}=[\bar{T}]^{\mathrm{T}}[C]_{\mathrm{p}}[\bar{T}],\qquad [\bar{e}]=[\bar{T}]^{\mathrm{T}}[e][R]\\
&\text{and}\qquad [\bar{\varepsilon}]=[R]^{-1}[\varepsilon][R].
\end{aligned}
\tag{21}
$$

For fibers coplanar with the vertical xz plane as shown in figure 2, $[\bar{T}]$ and $[R]$ are given by

$$
\begin{aligned}
[\bar{T}]^{-1} &= \begin{bmatrix}m^2 & 0 & n^2 & 0 & -mn & 0\\ 0 & 1 & 0 & 0 & 0 & 0\\ n^2 & 0 & m^2 & 0 & mn & 0\\ 0 & 0 & 0 & m & 0 & n\\ 2mn & 0 & -2mn & 0 & m^2-n^2 & 0\\ 0 & 0 & 0 & -n & 0 & m\end{bmatrix}\\
\text{and}\qquad [R] &= \begin{bmatrix}m & 0 & n\\ 0 & 1 & 0\\ -n & 0 & m\end{bmatrix}
\end{aligned}
\tag{22}
$$

while for fibers coplanar with the vertical yz plane these matrices are given by

$$
\begin{aligned}
[\bar{T}]^{-1} &= \begin{bmatrix}1 & 0 & 0 & 0 & 0 & 0\\ 0 & m^2 & n^2 & -mn & 0 & 0\\ 0 & n^2 & m^2 & mn & 0 & 0\\ 0 & 2mn & -2mn & m^2-n^2 & 0 & 0\\ 0 & 0 & 0 & 0 & m & -n\\ 0 & 0 & 0 & 0 & n & m\end{bmatrix}\\
\text{and}\qquad [R] &= \begin{bmatrix}1 & 0 & 0\\ 0 & m & n\\ 0 & -n & m\end{bmatrix}
\end{aligned}
\tag{23}
$$

in which $m = \cos\psi$ and $n = \sin\psi$. In the present work, the electric field is applied only in the z direction. Since the stress and the strain vectors for the shell and the PZC are defined differently (e.g. see equations (9) and (5)), constitutive equations (20) are rearranged as follows:

$$\begin{aligned} \{\sigma_b\}_{\rm p} &= [\bar{C}_b]_{\rm p}\{\in_b\}_b + [\bar{C}_{bs}]_{\rm p}\{\in_s\}_{\rm p} - \{e_b\}E_z, \\ \{\sigma_s\}_{\rm p} &= [\bar{C}_{bs}]_{\rm p}^{\rm T}\{\in_b\} + [\bar{C}_s]_{\rm p}\{\in_s\}_{\rm p} - \{e_s\}E_z, \\ \text{and} \qquad D_z &= \{e_b\}^{\rm T}\{\in_b\}_{\rm p} + \{e_s\}^{\rm T}\{\in_s\}_{\rm p} + \bar{\varepsilon}_{33}E_z. \end{aligned} \tag{24}$$

It follows from equations (24) that the transverse shear strains are coupled with the in-plane normal stresses and vice versa due to the orientation of the PZT fibers in the xz or yz plane, and the corresponding coupling matrices $[\bar{C}_{bs}]_{\rm p}$ are

$$\begin{aligned} [\bar{C}_{bs}]_{\rm p}^{\rm T} &= \begin{bmatrix} \bar{C}_{15} & \bar{C}_{25} & 0 & \bar{C}_{35} \\ 0 & 0 & \bar{C}_{46} & 0 \end{bmatrix}_{\rm p} \\ \text{or} \qquad [\bar{C}_{bs}]_{\rm p}^{\rm T} &= \begin{bmatrix} 0 & 0 & \bar{C}_{56} & 0 \\ \bar{C}_{14} & \bar{C}_{24} & 0 & \bar{C}_{34} \end{bmatrix}_{\rm p} \end{aligned} \tag{25}$$

respectively. For fibers coplanar with both xz and yz planes (i.e. $\psi = 0°$) this coupling matrix is a null matrix. Thus equations (24) and (25) reveal that the obliquely reinforced 1–3 PZC also acts as a shear actuator. In the augmented form of constitutive relations (24), the transformed elastic coefficient matrices $[\bar{C}_b]_{\rm p}$ and $[\bar{C}_s]_{\rm p}$, and the transformed effective piezoelectric constant matrices $\{e_b\}$ and $\{e_s\}$ are given by

$$\begin{aligned} [\bar{C}_b]_{\rm p} &= \begin{bmatrix} \bar{C}_{11} & \bar{C}_{12} & \bar{C}_{16} & \bar{C}_{13} \\ \bar{C}_{12} & \bar{C}_{22} & \bar{C}_{26} & \bar{C}_{23} \\ \bar{C}_{16} & \bar{C}_{26}^k & \bar{C}_{66} & \bar{C}_{36} \\ \bar{C}_{13} & \bar{C}_{23} & \bar{C}_{36} & \bar{C}_{33} \end{bmatrix}_{\rm p}, \\ [\bar{C}_s]_{\rm p} &= \begin{bmatrix} \bar{C}_{55} & \bar{C}_{45} \\ \bar{C}_{45} & \bar{C}_{44} \end{bmatrix}_{\rm p}, \qquad \{e_b\} = \begin{Bmatrix} \bar{e}_{31} \\ \bar{e}_{32} \\ \bar{e}_{36} \\ \bar{e}_{33} \end{Bmatrix} \\ \text{and} \qquad \{e_s\} &= \begin{Bmatrix} \bar{e}_{35} \\ \bar{e}_{34} \end{Bmatrix}. \end{aligned} \tag{26}$$

We note that the pyroelectric effect in a PZT has been neglected.

The principle of virtual work employed to derive governing equations of the system can be expressed as [24]

$$\begin{aligned} \int_\Omega \Big[& \delta\{\in_b\}_{\rm FG}^{\rm T}\{\sigma_b\}_{\rm FG} + \delta\{\in_s\}_{\rm FG}^{\rm T}\{\sigma_s\}_{\rm FG} + \delta\{\in_b\}_{\rm v}^{\rm T}\{\sigma_b\}_{\rm v} \\ & + \delta\{\in_s\}_{\rm v}^{\rm T}\{\sigma_s\}_{\rm v} + \delta\{\in_b\}_{\rm p}^{\rm T}\{\sigma_b\}_{\rm p} + \delta\{\in_s\}_{\rm p}^{\rm T}\{\sigma_s\}_{\rm p} \\ & - \delta E_z\bar{\varepsilon}_{33}E_z - \delta\{d_t\}^{\rm T}(\rho_{\rm FG} + \rho_{\rm v} + \rho_{\rm p})\{\ddot{d}_t\}\Big]\,{\rm d}\Omega \\ & - \int_A \delta\{d\}^{\rm T}\{f\}\,{\rm d}A = 0 \end{aligned} \tag{27}$$

in which δ is the symbol for the first variation, $\rho_{\rm v}$ and $\rho_{\rm p}$ are mass densities of the viscoelastic and the PZT materials, respectively, $\{f\}$ is the externally applied surface traction on surface area A and Ω represents the volume of the total domain. Here we have neglected the rotary inertia because the shell being studied is thin.

3. Solution of the problem by the FEM

The midsurface of the FG shell is discretized by eight-noded isoparametric elements. A typical FE is illustrated in figure 3(c) in which lengths a_e and b_e, respectively, in the axial and circumferential directions are given by $a_e = a/M$ and $b_e = 2\pi R/N$ with M and N equaling the number of elements along the length and the circumference of the FG shell. Following equation (4), the generalized displacement vector, associated with the ith ($i = 1, 2, 3 \ldots 8$) node of an element, is written as

$$\begin{aligned} \{d_{ti}\} &= [\,u_{0i} \quad v_{0i} \quad w_{0i}\,]^{\rm T} \qquad \text{and} \\ \{d_{ri}\} &= [\,\theta_{xi} \quad \theta_{yi} \quad \theta_{zi} \quad \phi_{xi} \quad \phi_{yi} \quad \phi_{zi} \quad \gamma_{xi} \quad \gamma_{yi} \quad \gamma_{zi}\,]^{\rm T}. \end{aligned} \tag{28}$$

The generalized displacement vector at a point in an element is expressed in terms of the generalized nodal displacement vectors $\{d_t^{\rm e}\}$ and $\{d_r^{\rm e}\}$ by

$$\{d_t\} = [N_t]\{d_t^{\rm e}\} \qquad \text{and} \qquad \{d_r\} = [N_r]\{d_r^{\rm e}\} \tag{29}$$

where

$$\begin{aligned} [N_t] &= [\,N_{t1} \quad N_{t2} \quad \cdots \quad N_{t8}\,]^{\rm T}, \\ [N_r] &= [\,N_{r1} \quad N_{r2} \quad \cdots \quad N_{r8}\,]^{\rm T}, \qquad N_{ti} = n_i I_t, \\ N_{ri} &= n_i I_r, \qquad \{d_t^{\rm e}\} = [\,\{d_{t1}^{\rm e}\}^{\rm T} \quad \{d_{t2}^{\rm e}\}^{\rm T} \quad \cdots \quad \{d_{t8}^{\rm e}\}^{\rm T}\,]^{\rm T} \\ \text{and} \qquad \{d_r^{\rm e}\} &= [\,\{d_{r1}^{\rm e}\}^{\rm T} \quad \{d_{r2}^{\rm e}\}^{\rm T} \quad \cdots \quad \{d_{r8}^{\rm e}\}^{\rm T}\,]^{\rm T} \end{aligned} \tag{30}$$

I_t and I_r are (3×3) and (9×9) identity matrices, respectively, and n_i is the shape function of natural coordinates associated with the ith node. Using relations (6)–(8) and (29), the strain vectors at a point in an element are expressed in terms of the nodal generalized displacement vectors as follows:

$$\begin{aligned} \{\in_b\}_{\rm FG} &= [B_{tb}]\{d_t^{\rm e}\} + [Z_1][B_{rb}]\{d_r^{\rm e}\}, \\ \{\in_b\}_{\rm v} &= [B_{tb}]\{d_t^{\rm e}\} + [Z_2][B_{rb}]\{d_r^{\rm e}\}, \\ \{\in_b\}_{\rm p} &= [B_{tb}]\{d_t^{\rm e}\} + [Z_3][B_{rb}]\{d_r^{\rm e}\}, \\ \{\in_s\}_{\rm FG} &= [B_{ts}]\{d_t^{\rm e}\} + [Z_4][B_{rs}]\{d_r^{\rm e}\}, \\ \{\in_s\}_{\rm v} &= [B_{ts}]\{d_t^{\rm e}\} + [Z_5][B_{rs}]\{d_r^{\rm e}\} \\ \text{and} \qquad \{\in_s\}_{\rm p} &= [B_{ts}]\{d_t^{\rm e}\} + [Z_6][B_{rs}]\{d_r^{\rm e}\}. \end{aligned} \tag{31}$$

The nodal strain–displacement matrices $[B_{tb}]$, $[B_{rb}]$, $[B_{ts}]$ and $[B_{rs}]$ are given by

$$\begin{aligned} [B_{tb}] &= [\,B_{tb1} \quad B_{tb2} \quad \cdots \quad B_{tb8}\,], \\ [B_{rb}] &= [\,B_{rb1} \quad B_{rb2} \quad \cdots \quad B_{rb8}\,], \\ [B_{ts}] &= [\,B_{ts1} \quad B_{ts2} \quad \cdots \quad B_{ts8}\,] \\ \text{and} \qquad [B_{rs}] &= [\,B_{rs1} \quad B_{rs2} \quad \cdots \quad B_{rs8}\,]. \end{aligned} \tag{32}$$

The submatrices $[B_{tb}]$, $[B_{rb}]$, $[B_{ts}]$ and $[B_{rs}]$ are given in the appendix. Upon substitution from equations (11), (15), (24) and (31) into equation (27) and recognizing that $E_z = -V/h_{\rm p}$ with V being the voltage difference applied across the PZT

layer, we obtain the following open loop equations of motion of an element:

$$[M^{\mathrm{e}}]\{\ddot{d}_t^{\mathrm{e}}\} + [K_{tt}^{\mathrm{e}}]\{d_t^{\mathrm{e}}\} + [K_{tr}^{\mathrm{e}}]\{d_r^{\mathrm{e}}\} = \{F_{tp}^{\mathrm{e}}\}V + \{F^{\mathrm{e}}\} + \{F_{Tb}^{\mathrm{e}}\} \tag{33}$$

$$[K_{rt}^{\mathrm{e}}]\{d_t^{\mathrm{e}}\} + [K_{rr}^{\mathrm{e}}]\{d_r^{\mathrm{e}}\} = \{F_{rp}^{\mathrm{e}}\}V + \{F_{Tr}^{\mathrm{e}}\}. \tag{34}$$

The element mass matrix $[M^{\mathrm{e}}]$, the stiffness matrices $[K_{tt}^{\mathrm{e}}]$, $[K_{tr}^{\mathrm{e}}]$ and $[K_{rr}^{\mathrm{e}}]$, the electro-elastic coupling vectors $\{F_{tp}^{\mathrm{e}}\}$ and $\{F_{rp}^{\mathrm{e}}\}$, the load vector $\{F^{\mathrm{e}}\}$, and the thermal load vectors $\{F_{Tb}^{\mathrm{e}}\}$ and $\{F_{Tr}^{\mathrm{e}}\}$ have expressions given below:

$$\begin{aligned}
&[M^{\mathrm{e}}] = \int_0^{a_e}\int_0^{b_e} \bar{m}[N_t]^{\mathrm{T}}[N_t]\,\mathrm{d}x\,\mathrm{d}y,\\
&\bar{m} = \int_{-h/2}^{h/2} \rho_{\mathrm{FG}}\,\mathrm{d}z + \rho_{\mathrm{v}}h_{\mathrm{v}} + \rho_{\mathrm{p}}h_{\mathrm{p}},\\
&[K_{tt}^{\mathrm{e}}] = [K_{tb}^{\mathrm{e}}] + [K_{ts}^{\mathrm{e}}] + [K_{tbs}^{\mathrm{e}}]_{pb} + [K_{tbs}^{\mathrm{e}}]_{ps},\\
&[K_{tr}^{\mathrm{e}}] = [K_{trb}^{\mathrm{e}}] + [K_{trs}^{\mathrm{e}}] + \tfrac{1}{2}([K_{trbs}^{\mathrm{e}}]_{pb} + [K_{rtbs}^{\mathrm{e}}]_{pb}^{\mathrm{T}}\\
&\qquad + [K_{trbs}^{\mathrm{e}}]_{ps} + [K_{rtbs}^{\mathrm{e}}]_{ps}^{\mathrm{T}}), \qquad [K_{rt}^{\mathrm{e}}] = [K_{tr}^{\mathrm{e}}]^{\mathrm{T}},\\
&[K_{rr}^{\mathrm{e}}] = [K_{rrb}^{\mathrm{e}}] + [K_{rrs}^{\mathrm{e}}] + [K_{rrbs}^{\mathrm{e}}]_{pb} + [K_{rrbs}^{\mathrm{e}}]_{ps},\\
&\{F_{tp}^{\mathrm{e}}\} = \{F_{tb}^{\mathrm{e}}\}_{\mathrm{p}} + \{F_{ts}^{\mathrm{e}}\}_{\mathrm{p}}, \qquad \{F_{rp}^{\mathrm{e}}\} = \{F_{rb}^{\mathrm{e}}\}_{\mathrm{p}} + \{F_{rs}^{\mathrm{e}}\}_{\mathrm{p}}\\
&\{F^{\mathrm{e}}\} = \int_0^{a_e}\int_0^{b_e} [N_t]^{\mathrm{T}}\{f\}\,\mathrm{d}x\,\mathrm{d}y,\\
&\{F_{Tb}^{\mathrm{e}}\} = \frac{1}{2}\int_0^{a_e}\int_0^{b_e}\int_{-h/2}^{h/2} [B_{tb}]^{\mathrm{T}}[C_b]_{\mathrm{FG}}\{\bar{\alpha}\}\Delta T\,\mathrm{d}z\,\mathrm{d}x\,\mathrm{d}y
\end{aligned} \tag{35}$$

and

$$\{F_{Tr}^{\mathrm{e}}\} = \frac{1}{2}\int_0^{a_e}\int_0^{b_e}\int_{-h/2}^{h/2} [B_{rb}]^{\mathrm{T}}[Z_1]^{\mathrm{T}}[C_b]_{\mathrm{FG}}\{\bar{\alpha}\}\Delta T\,\mathrm{d}z\,\mathrm{d}x\,\mathrm{d}y.$$

Stiffness matrices associated with the transverse shear strains are written separately so that the reduced-order integration rule can be easily employed to avoid the shear locking phenomenon in thin shells. The element stiffness matrices and the element electro-elastic coupling vectors in (35) corresponding to the bending–stretching deformations are given by

$$\begin{aligned}
[K_{tb}^{\mathrm{e}}] &= \int_0^{a_e}\int_0^{b_e} [B_{tb}]^{\mathrm{T}}[D_{tb}][B_{tb}]\,\mathrm{d}x\,\mathrm{d}y,\\
[K_{trb}^{\mathrm{e}}] &= \int_0^{a_e}\int_0^{b_e} [B_{trb}]^{\mathrm{T}}[D_{trb}][B_{rb}]\,\mathrm{d}x\,\mathrm{d}y,\\
[K_{rrb}^{\mathrm{e}}] &= \int_0^{a_e}\int_0^{b_e} [B_{rb}]^{\mathrm{T}}[D_{rrb}][B_{rb}]\,\mathrm{d}x\,\mathrm{d}y,\\
[K_{tbs}^{\mathrm{e}}]_{pb} &= \int_0^{a_e}\int_0^{b_e} [B_{tb}]^{\mathrm{T}}[D_{tbs}]_{\mathrm{p}}[B_{ts}]\,\mathrm{d}x\,\mathrm{d}y,\\
[K_{trbs}^{\mathrm{e}}]_{pb} &= \int_0^{a_e}\int_0^{b_e} [B_{tb}]^{\mathrm{T}}[D_{trbs}]_{\mathrm{p}}[B_{rs}]\,\mathrm{d}x\,\mathrm{d}y,\\
[K_{rtbs}^{\mathrm{e}}]_{pb} &= \int_0^{a_e}\int_0^{b_e} [B_{rb}]^{\mathrm{T}}[D_{rtbs}]_{\mathrm{p}}[B_{ts}]\,\mathrm{d}x\,\mathrm{d}y,\\
[K_{rrbs}^{\mathrm{e}}]_{pb} &= \int_0^{a_e}\int_0^{b_e} [B_{rb}]^{\mathrm{T}}[D_{rrbs}]_{\mathrm{p}}[B_{rs}]\,\mathrm{d}x\,\mathrm{d}y,\\
\{F_{tb}^{\mathrm{e}}\}_{\mathrm{p}} &= \int_0^{a_e}\int_0^{b_e} [B_{tb}]^{\mathrm{T}}\{D_{tb}\}_{\mathrm{p}}\,\mathrm{d}x\,\mathrm{d}y,\\
\{F_{rb}^{\mathrm{e}}\}_{\mathrm{p}} &= \int_0^{a_e}\int_0^{b_e} [B_{rb}]^{\mathrm{T}}\{D_{rb}\}_{\mathrm{p}}\,\mathrm{d}x\,\mathrm{d}y,
\end{aligned} \tag{36}$$

and those associated with the transverse shear deformations are given by

$$\begin{aligned}
[K_{ts}^{\mathrm{e}}] &= \int_0^{a_e}\int_0^{b_e} [B_{ts}]^{\mathrm{T}}[D_{ts}][B_{ts}]\,\mathrm{d}x\,\mathrm{d}y,\\
[K_{trs}^{\mathrm{e}}] &= \int_0^{a_e}\int_0^{b_e} [B_{ts}]^{\mathrm{T}}[D_{trs}][B_{rs}]\,\mathrm{d}x\,\mathrm{d}y,\\
[K_{rrs}^{\mathrm{e}}] &= \int_0^{a_e}\int_0^{b_e} [B_{rs}]^{\mathrm{T}}[D_{rrs}][B_{rs}]\,\mathrm{d}x\,\mathrm{d}y,\\
[K_{tbs}^{\mathrm{e}}]_{ps} &= \int_0^{a_e}\int_0^{b_e} [B_{ts}]^{\mathrm{T}}[D_{tbs}]_p^{\mathrm{T}}[B_{tb}]\,\mathrm{d}x\,\mathrm{d}y,\\
[K_{trbs}^{\mathrm{e}}]_{ps} &= \int_0^{a_e}\int_0^{b_e} [B_{ts}]^{\mathrm{T}}[D_{rtbs}]_p^{\mathrm{T}}[B_{rb}]\,\mathrm{d}x\,\mathrm{d}y,\\
[K_{rtbs}^{\mathrm{e}}]_{ps} &= \int_0^{a_e}\int_0^{b_e} [B_{rs}]^{\mathrm{T}}[D_{trbs}]_p^{\mathrm{T}}[B_{tb}]\,\mathrm{d}x\,\mathrm{d}y,\\
[K_{rrbs}^{\mathrm{e}}]_{ps} &= \int_0^{a_e}\int_0^{b_e} [B_{rs}]^{\mathrm{T}}[D_{rrbs}]_p^{\mathrm{T}}[B_{rb}]\,\mathrm{d}x\,\mathrm{d}y,\\
\{F_{ts}^{\mathrm{e}}\}_{\mathrm{p}} &= \int_0^{a_e}\int_0^{b_e} [B_{ts}]^{\mathrm{T}}\{D_{ts}\}_{\mathrm{p}}\,\mathrm{d}x\,\mathrm{d}y,\\
\{F_{rs}^{\mathrm{e}}\}_{\mathrm{p}} &= \int_0^{a_e}\int_0^{b_e} [B_{rs}]^{\mathrm{T}}\{D_{rs}\}_{\mathrm{p}}\,\mathrm{d}x\,\mathrm{d}y.
\end{aligned} \tag{37}$$

The rigidity matrices and rigidity vectors for electro-elastic coupling appearing in the above element matrices are given by

$$\begin{aligned}
[D_{tb}] &= [C_b]_{\mathrm{m}}\int_{-h/2}^{h/2}\left[1 + \left(\frac{E_{\mathrm{c}}}{E_{\mathrm{m}}} - 1\right)\left\{\frac{1}{2} + (-1)^k\frac{z}{h}\right\}^n\right]\mathrm{d}z\\
&\quad + [C_b]_{\mathrm{v}}h_{\mathrm{v}} + [\bar{C}_b]_{\mathrm{p}}h_{\mathrm{p}},\\
[D_{trb}] &= [C_b]_{\mathrm{m}}\int_{-h/2}^{h/2}\left[1 + \left(\frac{E_{\mathrm{c}}}{E_{\mathrm{m}}} - 1\right)\left\{\frac{1}{2} + (-1)^k\frac{z}{h}\right\}^n\right]\\
&\quad \times [Z_1]\,\mathrm{d}z + \int_{h/2}^{h_1}[C_b]_{\mathrm{v}}[Z_2]\,\mathrm{d}z + \int_{h_1}^{h_2}[\bar{C}_b]_{\mathrm{p}}[Z_3]\,\mathrm{d}z,\\
[D_{rrb}] &= \int_{-h/2}^{h/2}\left[1 + \left(\frac{E_{\mathrm{c}}}{E_{\mathrm{m}}} - 1\right)\left\{\frac{1}{2} + (-1)^k\frac{z}{h}\right\}^n\right]\\
&\quad \times [Z_1]^{\mathrm{T}}[C_b]_{\mathrm{m}}[Z_1]\,\mathrm{d}z + \int_{h/2}^{h_1}[Z_2]^{\mathrm{T}}[C_b]_{\mathrm{v}}[Z_2]\,\mathrm{d}z\\
&\quad + \int_{h_1}^{h_2}[Z_3]^{\mathrm{T}}[\bar{C}_b]_{\mathrm{p}}[Z_3]\,\mathrm{d}z\\
[D_{ts}] &= [C_s]_{\mathrm{m}}\int_{-h/2}^{h/2}\left[1 + \left(\frac{E_{\mathrm{c}}}{E_{\mathrm{m}}} - 1\right)\left\{\frac{1}{2} + (-1)^k\frac{z}{h}\right\}^n\right]\mathrm{d}z\\
&\quad + [C_s]_{\mathrm{v}}h_{\mathrm{v}} + [\bar{C}_s]_{\mathrm{p}}h_{\mathrm{p}},
\end{aligned}$$

$$[D_{trs}] = [C_s]_{\mathrm{m}} \int_{-h/2}^{h/2} \left[1 + \left(\frac{E_{\mathrm{c}}}{E_{\mathrm{m}}} - 1\right)\left\{\frac{1}{2} + (-1)^k \frac{z}{h}\right\}^n\right] \times [Z_4]\,\mathrm{d}z + \int_{h/2}^{h_1} [C_s]_{\mathrm{v}}[Z_5]\,\mathrm{d}z + \int_{h_1}^{h_2} [\bar{C}_s]_{\mathrm{p}}[Z_6]\,\mathrm{d}z,$$

$$[D_{rrs}] = \int_{-h/2}^{h/2} \left[1 + \left(\frac{E_{\mathrm{c}}}{E_{\mathrm{m}}} - 1\right)\left\{\frac{1}{2} + (-1)^k \frac{z}{h}\right\}^n\right] \times [Z_4]^{\mathrm{T}}[C_s]_{\mathrm{m}}[Z_4]\,\mathrm{d}z + \int_{h/2}^{h_1} [Z_5]^{\mathrm{T}}[C_s]_{\mathrm{v}}[Z_5]\,\mathrm{d}z + \int_{h_1}^{h_2} [Z_6]^{\mathrm{T}}[\bar{C}_s]_{\mathrm{p}}[Z_6]\,\mathrm{d}z,$$

$$[D_{tbs}]_{\mathrm{p}} = \int_{h_1}^{h_2} [\bar{C}_{bs}]_{\mathrm{p}}\,\mathrm{d}z,$$

$$[D_{trbs}]_{\mathrm{p}} = \int_{h_1}^{h_2} [\bar{C}_{bs}]_{\mathrm{p}}[Z_6]\,\mathrm{d}z,$$

$$[D_{rtbs}]_{\mathrm{p}} = \int_{h_1}^{h_2} [Z_3]^{\mathrm{T}}[\bar{C}_{bs}]_{\mathrm{p}}\,\mathrm{d}z,$$

$$[D_{rrbs}]_{\mathrm{p}} = \int_{h_1}^{h_2} [Z_3]^{\mathrm{T}}[\bar{C}_{bs}]_{\mathrm{p}}[Z_6]\,\mathrm{d}z,$$

$$\{D_{tb}\}_{\mathrm{p}} = -\int_{h_1}^{h_2} \{\bar{e}_b\}/h_{\mathrm{p}}\,\mathrm{d}z$$

$$\{D_{rb}\}_{\mathrm{p}} = -\int_{h_1}^{h_2} [Z_3]^{\mathrm{T}}\{\bar{e}_b\}/h_{\mathrm{p}}\,\mathrm{d}z,$$

$$\{D_{ts}\}_{\mathrm{p}} = -\int_{h_1}^{h_2} \{\bar{e}_s\}/h_{\mathrm{p}}\,\mathrm{d}z,$$

$$\{D_{rs}\}_{\mathrm{p}} = -\int_{h_1}^{h_2} [Z_6]^{\mathrm{T}}\{\bar{e}_s\}/h_{\mathrm{p}}\,\mathrm{d}z. \tag{38}$$

For an element not contacting the ACLD patch, the electro-elastic coupling matrices are null matrices and the element stiffness matrices will be real. The element equations of motion are assembled to obtain the following open loop global equations of motion:

$$[M]\{\ddot{X}\} + [K_{tt}]\{X\} + [K_{tr}]\{X_r\} = \sum_{j=1}^{q} \{F_{tp}^j\}V^j + \{F\} + \{F_{Tb}\} \tag{39}$$

and

$$[K_{rt}]\{X\} + [K_{rr}]\{X_r\} = \sum_{j=1}^{q} \{F_{rp}^j\}V^j + \{F_{Tr}\} \tag{40}$$

where $[M]$ is the global mass matrix, $[K_{tt}]$, $[K_{tr}]$ and $[K_{rr}]$ are the global stiffness matrices, $\{F_{tp}\}$ and $\{F_{rp}\}$ are the global electro-elastic coupling vectors, $\{X\}$ and $\{X_r\}$ are the global nodal generalized displacement vectors, $\{F\}$ is the global nodal force vector, $\{F_{Tb}\}$ and $\{F_{Tr}\}$ are the global nodal thermal load vectors, q is the number of patches and V^j is the voltage difference applied to the jth patch. Since the stiffness matrices of an element augmented with the ACLD treatment are complex, the global stiffness matrices become complex and the energy dissipation characteristics of the overall plate are attributed to the imaginary parts of these matrices. Hence, the global equations of motion as derived above also represent the passive (uncontrolled) constrained layer damping of the substrate plate when the constraining layer is not subjected to any control voltage following a derivative control law.

4. Active damping

In the active control strategy, the constraining layer of each patch is activated with a control voltage proportional to the transverse speed of a point, and the applied electric field opposes the velocity of the point. The exact location of the point in the ACLD patch is described in the next section. Thus the control voltage for each patch can be expressed in terms of the time derivative of the global nodal degrees of freedom as follows:

$$V^j = -k_d^j \dot{w} = -k_d^j [U_t^j]\{\dot{X}\} - k_d^j (h/2)[U_r^j]\{\dot{X}_r\} \tag{41}$$

where k_d^j is the control gain for the jth patch, and $[U_t^j]$ and $[U_r^j]$ are unit vectors along the transverse velocity of the point. Substituting from equation (39) into equations (37) and (38), the final equations of motion governing the closed loop dynamics of the overall FG shell/ACLD system with the shell only subjected to a temperature gradient in the thickness direction can be written as follows:

$$[M]\{\ddot{X}\} + \sum_{j=1}^{m} k_d^j \{F_{tp}^j\}[U_t^j]\{\dot{X}\} + \sum_{j=1}^{m} k_d^j (h/2)\{F_{tp}^j\}[U_r^j]\{\dot{X}_r\} + [K_{tt}]\{X\} + [K_{tr}]\{X_r\} = \{F\} + \{F_{Tb}\} \tag{42}$$

and

$$\sum_{j=1}^{m} k_d^j \{F_{rp}^j\}[U_t^j]\{\dot{X}\} + \sum_{j=1}^{m} k_d^j (h/2)\{F_{rp}^j\}[U_r^j]\{\dot{X}_r\} + [K_{rt}]\{X\} + [K_{rr}]\{X_r\} = \{F_{Tr}\}. \tag{43}$$

5. Results and discussion

A thin cantilevered circular cylindrical FG shell integrated with two patches of ACLD treatment is considered for computing numerical results. As shown in figure 1, the patches are placed 180° apart from each other with their one end surface at the clamped edge of the shell. These locations of the patches cause maximum energy dissipation in the first two ((1, 2) and (1, 1)) modes of vibration [26]. The length of each patch equals 75% of the length of the FG shell while the width of the patch is one-sixth of the circumference of the shell. The constraining layer of the ACLD treatment is a PZT-5H/spur composite with 60% volume fraction of PZT fibers. Effective material properties of this vertically reinforced 1–3 PZC ($\psi = 0°$), computed following the procedure of Smith and Auld [29], are

$$C_{11} = 9.29\ \mathrm{GPa}, \qquad C_{12} = 6.18\ \mathrm{GPa},$$

$$C_{13} = 6.05\ \mathrm{GPa}, \qquad C_{33} = 35.44\ \mathrm{GPa},$$

$$C_{23} = C_{13},$$

$$C_{44} = 1.58\ \mathrm{GPa}, \qquad C_{66} = 1.54\ \mathrm{GPa},$$

Table 1. Convergence of the first two computed natural frequencies (Hz).

FE mesh $N \times M$	1st mode (1, 2)	2nd mode (1, 1)
8×6	208.58	288.15
10×6	204.34	284.66
12×6	204.32	284.57
12×8	204.31	284.56

$$C_{55} = C_{44}, \qquad e_{31} = -0.1902 \text{ C m}^{-2}, \qquad e_{32} = e_{31},$$

$$e_{33} = 18.4107 \text{ C m}^{-2}, \qquad e_{24} = 0.004 \text{ C m}^{-2},$$

$$e_{15} = e_{24}.$$

Using equations (21)–(23) and the above listed effective material properties for $\psi = 0°$, the effective material properties of obliquely reinforced 1–3 PZC are computed. The FG shell is composed of aluminum (Al) and alumina (Al_2O_3) and values of their material parameters are

Aluminum: $E_m = 70$ GPa, $\kappa_m = 204$ W m^{-1} K^{-1},

$\alpha_m = 23.0 \times 10^{-6}$ °C^{-1} and $\rho_m = 2707$ kg m^{-3}

Alumina: $E_c = 380$ GPa, $\kappa_c = 10.4$ W m^{-1} K^{-1},

$\alpha_c = 7.4 \times 10^{-6}$ °C^{-1} and $\rho_c = 3800$ kg m^{-3}.

Poisson's ratio of both constituent materials is taken as 0.3. The complex shear modulus, Poisson's ratio and the mass density of the viscoelastic constrained layer are $20(1 + i)$ MN m^{-2}, 0.49 and 1140 kg m^{-3}, respectively [23]. Unless otherwise mentioned, the thicknesses of the substrate FG shell, the viscoelastic layer and the PZT layer are 4, 1 and 1 mm, respectively. The length and the value of (R/h) for the substrate FG shell are 1 m and 50, respectively. Also, unless otherwise mentioned, temperatures of the ceramic-rich and the metal-rich surfaces are 400 and 300 K, respectively, and the ambient temperature is 300 K. Stiffness matrices corresponding to the bending deformations have been evaluated by using the 2×2 Gauss quadrature rule, and those corresponding to the transverse shear deformations have been computed with a one-point integration rule while the value of shear correction factor is considered as 5/6. We have adopted the same value of the shear correction factor as that for a flat plate made of a homogeneous material.

Table 1 lists values of natural frequencies of the system with $n = 1$ and $k = 1$ in equation (10) for the first two modes, namely (1, 2) and (1, 1), of vibration for different FE meshes given in the first column of the table. Uniform FE meshes with N elements in the circumferential direction and M elements in the axial direction have been employed in the convergence study. It is clear that the FE mesh with $N = 12$ and $M = 8$ gives converged values of these two frequencies. This mesh is employed in the subsequent work reported below.

In order to verify the FE code, we set $n = 10$, $k = 1$ in equation (10) so that the material of the shell becomes almost homogeneous, taking the constraining layer of the ACLD patch to be made of PVDF (polyvinylidene fluoride), and the geometrical parameters and material properties of the overall shell to be the same as those of the shell studied by Ray *et al* [25]. Computed natural frequencies of this system held at a uniform temperature are compared in table 2 with those listed in [25]. It is clear that the two sets of results agree well with each other.

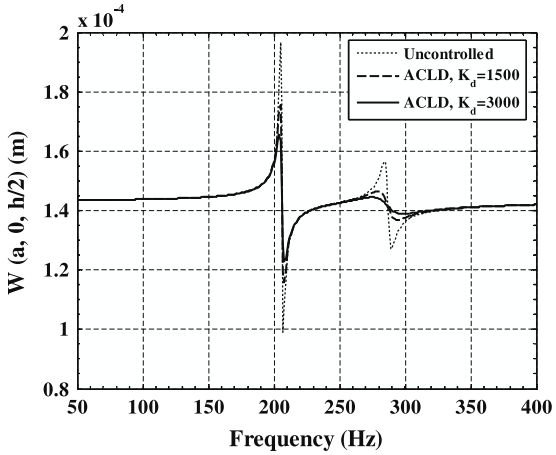

Figure 4. Frequency response functions for the transverse displacement w $(a/2, 0, h/2)$ of a point at the free end of the FG shell ($k = 1, n = 1, \psi = 0°, T_c = 400$ K, $T_m = 300$ K).

Table 2. Comparison of the first two natural frequencies (Hz) of the overall shell ($n = 10, k = 1$) when it is degenerated to the homogeneous isotropic shell studied by Ray *et al* [25] in the absence of thermal effects.

Source	Mode (1, 2)	Mode (1, 1)
Present FEM	53.08	114.21
Experiment [25]	51.2	113
FEM [25]	54.06	113.62

We now investigate the performance of the 1–3 PZC by finding the frequency response of the FG shell with the ACLD patch. Equations (42) and (43) are rewritten to compute the frequency response functions when the shell is excited by a time harmonic force of 4 N amplitude applied at the point $(a, 0, h/2)$, i.e. at the free end of the substrate FG shell. The electric field applied to the first patch is proportional to the negative of the velocity of the point $(0.65a, 0, -h/2)$ and that applied to the other patch is proportional to the negative of the velocity of the point $(0.65a, s/2, -h/2)$, where s is the length of the mid-plane perimeter of the shell. The control gains are arbitrarily chosen so that the first few modes are efficiently controlled. Also, unless otherwise mentioned, the patches are integrated with the softest surface (metal-rich, $k = 1$) of the FG shell while fibers are vertically reinforced ($\psi = 0°$) in the constraining layer of the patches. Figure 4 illustrates the frequency response functions for the transverse displacement w of the point $(a, 0, h/2)$ with the shell subjected to a temperature gradient ($T_c = 400$ K, $T_m = 300$ K) across its thickness when the patches are and are not actively controlled. The variation with the frequency of excitation of

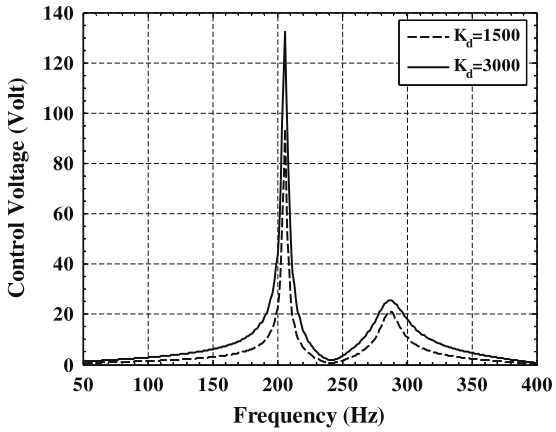

Figure 5. Variation of the control voltage with the frequency of excitation for the active damping of the FG shell ($k = 1$, $n = 1$, $\psi = 0°$, $T_c = 400$ K, $T_m = 300$ K).

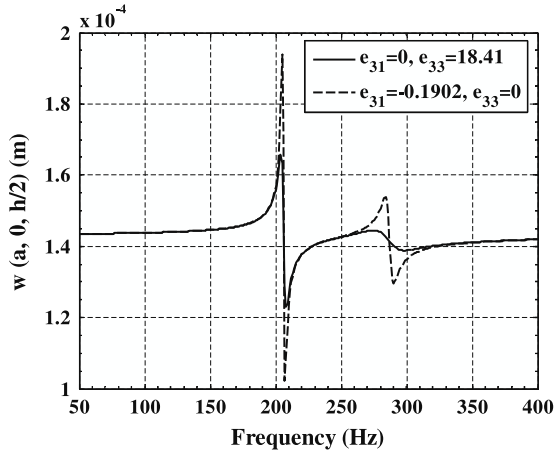

Figure 6. Comparison of vertical and in-plane actuations induced by the constraining layer of the ACLD patches bonded to the FG shell (gain = 3000, $k = 1$, $n = 1$, $\psi = 0°$, $T_c = 400$ K, $T_m = 300$ K).

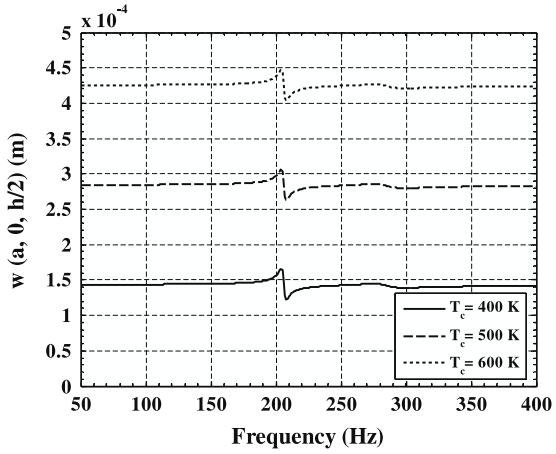

Figure 7. Frequency response functions for the transverse displacement w $(a, 0, h/2)$ of a point at the free end of the FG shell subjected to different temperature gradients ($k = 1$, $n = 1$, $\psi = 0°$, $T_m = 300$ K).

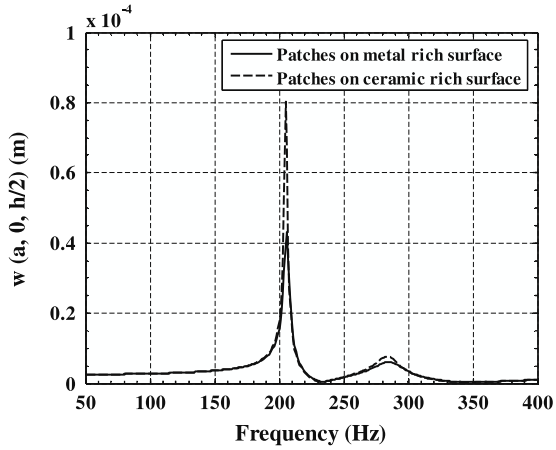

Figure 8. Comparison of the active responses of the FG shell in the absence of temperature gradients ($T_c = T_m = 300$ K) with patches bonded to the softest and the stiffest surface of the shell (gain = 3000, $n = 1$, $\psi = 0°$).

the required control voltage applied to each patch is exhibited in figure 5. Results plotted in figure 4 clearly reveal that the activated patches significantly attenuate the amplitude of vibrations, and enhance damping characteristics of the system over the uncontrolled system. The maximum control voltage required to achieve this damping is quite low as illustrated in figure 5.

In order to investigate the contribution of the vertical actuation in improving the damping characteristics of the heat conducting FG shell, its active control responses for a gain of 3000 are plotted in figure 6 with zero and non-zero values of e_{33} and e_{31}. When $e_{31} = 0$ and $e_{33} \neq 0$, the vertical actuation of the active constraining layer of the ACLD treatment increases transverse shear deformations of the viscoelastic constrained layer over the passively controlled case, resulting in improved damping of the shell. On the other hand, when $e_{33} = 0$ and $e_{31} \neq 0$, the in-plane actuation of the active constraining layer increases transverse shear deformations of the viscoelastic core leading to improved overall damping of the shell. It is evident from results exhibited in figure 6 that the contribution of e_{33} is significantly more than that of e_{31} in controlling modes displayed in figure 4. Similar results are obtained for patches with PZT fibers obliquely oriented ($0° \leqslant \psi \leqslant 45°$) in the constraining layer, and are omitted for the sake of brevity. Frequency response functions for transverse displacement w of the point $(a, 0, h/2)$ with the shell subjected to different temperature gradients are plotted in figure 7. It is apparent from these results that, for higher values of the temperature gradient, the deflection of the free end of the shell increases but the ACLD patches still effectively control vibrations of the shell.

In figure 8 we compare the closed loop response of the FG shell in the absence of a thermal gradient across its thickness when the patches are attached to the softest surface (metal-rich, $k = 1$) of the shell with that when the patches are integrated with the stiffest surface (ceramic-rich, $k = 2$) of the shell; the corresponding voltage differences are compared in figure 9. It can be concluded from these

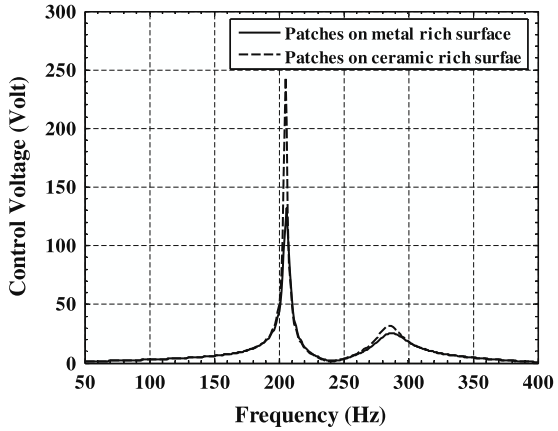

Figure 9. Comparison of the control voltages for obtaining active responses when patches are bonded to the softest and the stiffest surface of the FG shell (gain = 3000, $n = 1$, $\psi = 0°$).

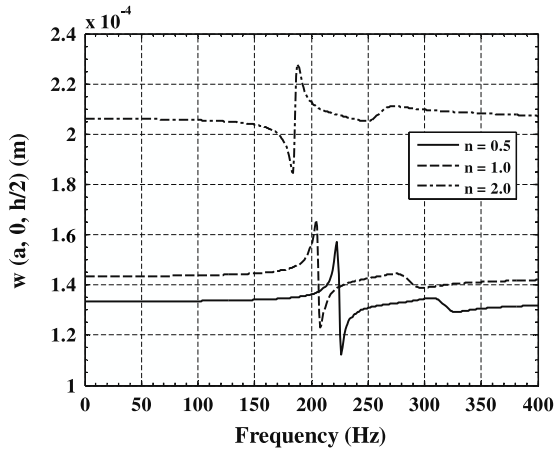

Figure 10. Effect of the variation of the power law exponent n on the performance of the patches for active damping of the FG shell (gain = 3000, $k = 1$, $\psi = 0°$, $T_c = 400$ K, $T_m = 300$ K).

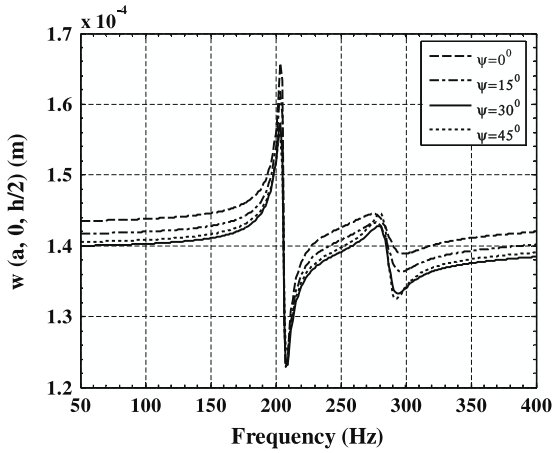

Figure 11. Effect of the variation of the fiber orientation ψ on the performance of the ACLD patches bonded to the cantilevered FG shell when the PZT fibers in the constraining layer are coplanar with the xz plane (gain = 3000, $k = 1$, $n = 1$, $T_c = 400$ K, $T_m = 300$ K).

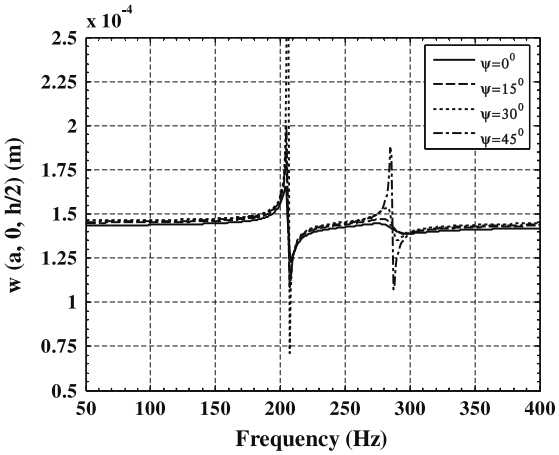

Figure 12. Effect of the variation of the fiber orientation ψ on the performance of the ACLD patches bonded to the cantilevered FG shell when the PZT fibers in the constraining layer are coplanar with the yz plane (gain = 3000, $k = 1$, $n = 1$, $T_c = 400$ K, $T_m = 300$ K).

results that the active patches when bonded to the softest surface of the FG shell cause more attenuation of vibrations (figure 8) with less control voltage (figure 9) than patches attached to the stiffest surface of the shell. This indicates that patches bonded to the softest surface of the FG shell perform better than those bonded to the stiffest surface of the shells. The substrate FG shell is basically antisymmetric because material properties vary across its thickness. Consequently, its bending and stretching deformations are coupled. This coupling is reduced if patches are attached to the softest surface of the substrate FG shell. This phenomenon is also observed in exact solutions [21] and active damping of smart FG plates [33].

The effect of varying the exponent n in equation (10) on the frequency response spectrum is exhibited in figure 10. Since the effective modulus at any point of the substrate FG shell increases with a decrease in the value of n, natural frequencies of the overall shell increase. We note that, with an increase in the value of n, the frequency corresponding to the maximum value of w decreases.

The effect of varying the PZT fiber orientation angle ψ in vertical xz and yz planes on the performance of patches has also been studied. The maximum value of ψ in the commercially available obliquely reinforced 1–3 PZC is 45° (see footnote 1); hence we vary ψ between 0° and 45°. In order to clearly decipher the plots, responses corresponding to only four values of ψ are included in figures 11 and 12. These results imply that the maximum attenuation due to these patches occurs for $\psi = 30°$ with fibers in the xz plane. Furthermore, PZT fibers oriented in the vertical xz plane perform better than fibers oriented in the vertical yz plane.

6. Conclusions

We have investigated the performance of a vertically and obliquely reinforced 1–3 piezocomposite as a material for the constraining layer of an ACLD treatment by studying vibration control of an FG shell with ACLD patches. The

shell is comprised of two materials with their volume fractions varying only in the thickness direction. The shell is also subjected to a temperature gradient while the temperature is assumed to vary only along the shell thickness. Three-dimensional deformations of the system are analyzed by using the first-order shear deformation theory modified to include the effect of transverse normal strains. Thus both in-plane and transverse actuations of the constraining layer of the ACLD patches can be utilized for active damping of shells. An approximate solution of the governing equations is found by the finite element method using an eight-noded serendipity element. The frequency response of an FG shell indicates that the active constraining layer of the ACLD treatment significantly enhances the damping of the shell over the passive damping. The contribution of the vertical actuation of the constraining layer towards damping of the shell's vibrations significantly exceeds that of the in-plane actuation of the constraining layer. For a cantilevered shell, the performance of the ACLD patches is the maximum for an obliquely reinforced 1–3 piezocomposite with the fiber orientation angle $\psi = 30°$ in the vertical xz plane. Also, the obliquely reinforced 1–3 piezocomposite with fibers in the vertical xz plane performs better than the one with fibers in the vertical yz plane.

Acknowledgments

RCB's work was partially supported by the Office of Naval Research grant N00014-06-1-0567 to Virginia Polytechnic Institute and State University with Dr Y D S Rajapakse as the program manager. Views expressed in the paper are those of the authors and not of the funding agency nor of their institutions.

Appendix

Matrices $[Z_1]$, $[Z_2]$, $[Z_3]$, $[Z_4]$, $[Z_5]$ and $[Z_6]$ appearing in equations (6) and (7) are given by

$$[Z_1] = [\,[\bar{Z}_1] \quad \tilde{o} \quad \tilde{o}\,], \qquad [Z_2] = [\,(h/2)I \quad [\bar{Z}_2] \quad \tilde{o}\,],$$

$$[Z_3] = [\,(h/2)I \quad h_v I \quad [\bar{Z}_3]\,],$$

$$[Z_4] = [\,[\overline{Z}_4] \quad \bar{o} \quad \bar{o} \quad z\bar{I} \quad \bar{o} \quad \bar{o}\,],$$

$$[Z_5] = [\,\tfrac{h}{2R} I_1 \quad [\overline{Z}_5] \quad \bar{o} \quad (h/2)\bar{I} \quad (z-h/2)\bar{I} \quad \bar{o}\,],$$

$$[Z_6] = [\,\tfrac{h}{2R} I_1 \quad \tfrac{h_v}{R} I_1 \quad \overline{Z}_6 \quad (h/2)\bar{I} \quad h_v\bar{I} \quad (z-h_{N+2})\bar{I}\,],$$

in which

$$[\bar{Z}_1] = \begin{bmatrix} z & 0 & 0 & 0 \\ 0 & z & 0 & \frac{z}{R} \\ 0 & 0 & z & 0 \\ 0 & 0 & 0 & 1 \end{bmatrix},$$

$$[\bar{Z}_2] = \begin{bmatrix} (z-h/2) & 0 & 0 & 0 \\ 0 & (z-h/2) & 0 & \frac{(z-h/2)}{R} \\ 0 & 0 & (z-h/2) & 0 \\ 0 & 0 & 0 & 1 \end{bmatrix},$$

$$[\bar{Z}_3] = \begin{bmatrix} (z-h_{N+2}) & 0 & 0 & 0 \\ 0 & (z-h_{N+2}) & 0 & 0 \\ 0 & 0 & (z-h_{N+2}) & (z-h_{N+2})/R \\ 0 & 0 & 0 & 1 \end{bmatrix},$$

$$[\overline{Z}_4] = \begin{bmatrix} 1 & 0 \\ 0 & \frac{z}{R} \end{bmatrix}, \qquad [\overline{Z}_5] = \begin{bmatrix} 1 & 0 \\ 0 & 1-(z-h/2)/R \end{bmatrix},$$

$$[\overline{Z}_6] = \begin{bmatrix} 1 & 0 \\ 0 & 1-(z-h_{N+2})/R \end{bmatrix},$$

$$I = \begin{bmatrix} 1 & 0 & 0 & 0 \\ 0 & 1 & 0 & \frac{1}{R} \\ 0 & 0 & 1 & 0 \\ 0 & 0 & 0 & 0 \end{bmatrix}, \qquad I_1 = \begin{bmatrix} 0 & 0 \\ 0 & -1 \end{bmatrix},$$

$$\bar{I} = \begin{bmatrix} 1 & 0 \\ 0 & 1 \end{bmatrix}, \qquad \bar{o} = \begin{bmatrix} 0 & 0 \\ 0 & 0 \end{bmatrix}$$

and $$\tilde{o} = \begin{bmatrix} \bar{o} & \bar{o} \\ \bar{o} & \bar{o} \end{bmatrix}.$$

Submatrices B_{tbi}, B_{tsi}, B_{rbi} and B_{rsi} appearing in equation (31) have the following expressions:

$$B_{tbi} = \begin{bmatrix} \frac{\partial n_i}{\partial x} & 0 & 0 \\ 0 & \frac{\partial n_i}{\partial y} & 1/R \\ \frac{\partial n_i}{\partial y} & \frac{\partial n_i}{\partial x} & 0 \\ 0 & 0 & 0 \end{bmatrix},$$

$$B_{rbi} = \begin{bmatrix} \bar{B}_{rbi} & \widehat{0} & \widehat{0} \\ \widehat{0} & \bar{B}_{rbi} & \widehat{0} \\ \widehat{0} & \widehat{0} & \bar{B}_{rbi} \end{bmatrix},$$

$$\bar{B}_{rbi} = \begin{bmatrix} \frac{\partial n_i}{\partial x} & 0 & 0 \\ 0 & \frac{\partial n_i}{\partial y} & 0 \\ \frac{\partial n_i}{\partial y} & \frac{\partial n_i}{\partial x} & 0 \\ 0 & 0 & 1 \end{bmatrix},$$

$$B_{tsi} = \begin{bmatrix} 0 & 0 & \frac{\partial n_i}{\partial x} \\ 0 & -1/R & \frac{\partial n_i}{\partial y} \end{bmatrix},$$

$$B_{rsi} = \begin{bmatrix} \widehat{I} & \breve{0} & \breve{0} \\ \breve{0} & \widehat{I} & \breve{0} \\ \breve{0} & \breve{0} & \widehat{I} \\ \bar{B}_{rsi} & \breve{0} & \breve{0} \\ \breve{0} & \bar{B}_{rsi} & \breve{0} \\ \breve{0} & \breve{0} & \bar{B}_{rsi} \end{bmatrix},$$

$$\bar{B}_{rsi} = \begin{bmatrix} 0 & 0 & \frac{\partial n_i}{\partial x} \\ 0 & 0 & \frac{\partial n_i}{\partial y} \end{bmatrix} \quad \text{and} \quad \widehat{I} = \begin{bmatrix} 1 & 0 & 0 \\ 0 & 1 & 0 \end{bmatrix};$$

where $\widehat{0}$ and $\breve{0}$ are (3×3) and (2×3) null matrices, respectively.

References

[1] Koizumi M 1993 Concept of FGM *Ceram. Trans.* **34** 3–10
[2] Aboudi J, Pindera M J and Arnold S M 1996 Thermoelastic theory for the response of materials functionally graded in two directions *Int. J. Solids Struct.* **33** 931–66

[3] Loy C T, Lam K Y and Reddy J N 1999 Vibration of functionally graded cylindrical shells *Int. J. Mech. Sci.* **41** 309–24
[4] Vel S S and Batra R C 2002 Exact solution for thermoelastic deformations of functionally graded thick rectangular plates *AIAA J.* **40** 1421–33
[5] Woo J and Meguid S A 2001 Nonlinear analysis of functionally graded plates and shallow shells *Int. J. Solids Struct.* **38** 7409–21
[6] Vel S S and Batra R C 2003 Three-dimensional analysis of transient thermal stresses in functionally graded plates *Int. J. Solids Struct.* **40** 7181–96
[7] Park J S and Kim J H 2006 Thermal postbuckling and vibration analyses of functionally graded plates *J. Sound Vib.* **289** 67–84
[8] Bailey T and Hubbard J E 1985 Distributed piezoelectric polymer active vibration control of a cantilever beam *J. Guid. Control Dyn.* **8** 605–11
[9] Miller S E and Hubbard J E 1987 Observability of a Bernoulli–Euler beam using PVF_2 as a distributed sensor *MIT Draper Laboratory Report*
[10] Baz A and Poh S 1988 Performance of an active control system with piezoelectric actuators *J. Sound Vib.* **126** 327–43
[11] Stöbener U and Gaul L 2000 Modal vibration control for PVDF coated plates *J. Intell. Mater. Syst. Struct.* **11** 283–93
[12] Lin J C and Nien M H 2005 Adaptive control of a composite cantilever beam with piezoelectric damping-modal actuators/sensors *Compos. Struct.* **70** 170–6
[13] Ootao Y and Tanigawa Y 2000 Three-dimensional transient thermoelasticity in functionally graded rectangular plate bonded to a piezoelectric plate *Int. J. Solids Struct.* **37** 4377–401
[14] Ootao Y and Tanigawa Y 2001 Control of the transient thermoelastic displacement of a functionally graded rectangular plate bonded to a piezoelectric plate due to nonuniform heating *Acta Mech.* **148** 17–33
[15] Wang B L and Noda N 2001 Design of a smart functionally graded thermopiezoelectric composite structure *Smart Mater. Struct.* **10** 189–93
[16] He X Q, Ng T Y, Sivashanker S and Liew K M 2001 Active control of FGM plates with integrated piezoelectric sensors and actuators *Int. J. Solids Struct.* **38** 1641–55
[17] Liew K M, He X Q, Ng T Y and Kitipornchai S 2003 Finite element piezothermoelasticity analysis and the active control of FGM plates with integrated piezoelectric sensors and actuators *Comput. Mech.* **31** 350–8
[18] Yang J, Kitipornchi S and Liew K M 2003 Large amplitude vibration of thermo-electro-mechanically stressed FGM laminated plates *Comput. Methods Appl. Mech. Eng.* **192** 3861–85
[19] Yang J, Kitipornchai S and Liew K M 2004 Non-linear analysis of thermo-electro-mechanical behavior of shear deformable FGM plates with piezoelectric actuators *Int. J. Numer. Methods Eng.* **59** 1605–32
[20] Shen H S 2005 Post buckling of FGM plates with piezoelectric actuators under thermo-electro-mechanical loadings *Int. J. Solids Struct.* **42** 6101–21
[21] Ray M C and Sachade H M 2006 Exact solutions for the functionally graded plates integrated with a layer of piezoelectric fiber-reinforced composite *ASME J. Appl. Mech.* **73** 622–32
[22] Baz A and Ro J 1995 vibration control of plates with active constrained layer damping *Smart Mater. Struct.* **5** 272–80
[23] Chantalakhana C and Stanway R 2001 Active constrained layer damping of clamped–clamped plate vibrations *J. Sound Vib.* **241** 755–77
[24] Jeung Y S and Shen I Y 2001 Development of isoparametric, degenerate constrained layer treatment for plate and shell structures *AIAA J.* **39** 1997–2005
[25] Ray M C, Oh J and Baz A 2001 Active constrained layer damping of thin cylindrical shells *J. Sound Vib.* **240** 921–35
[26] Ray M C and Reddy J N 2004 Optimal control of thin circular cylindrical shells using active constrained layer damping treatment *Smart Mater. Struct.* **13** 64–72
[27] Langote P K and Seshu P 2005 Experimental studies on active vibration control of a beam using hybrid active/passive constrained layer damping treatments *ASME J. Vib. Acoust.* **127** 515–8
[28] Chetwynd D, Lew T L, Worden K and Rongong J A 2007 Damage detection in an aluminium plate with an active constrained layer damping treatment *Key Eng. Mater.* **347** 205–12
[29] Smith W A and Auld B A 1991 Modeling 1–3 composite piezoelectrics: thickness mode oscillations *IEEE Trans. Ultrason. Ferroelectr. Freq. Control* **31** 40–7
[30] Hellen L C, Kun L and Chung L C 2003 Piezoelectric ceramic fiber/epoxy 1–3 composite for high frequency ultrasonic transducer application *Mater. Sci. Eng.* B **99** 29–35
[31] Ray M C and Prodhan A K 2006 The performance of vertically reinforced 1–3 piezoelectric composites in active damping of smart structures *Smart Mater. Struct.* **15** 631–41
[32] Ray M C and Prodhan A K 2007 On the use of vertically reinforced 1–3 piezoelectric composites for hybrid damping of laminated composite plates *Mech. Adv. Mater. Struct.* **14** 245–62
[33] Ray M C and Batra R C 2007 Performance of vertically/obliquely reinforced 1–3 piezoelectric composites for active damping of functionally graded plates *AIAA J.* **45** 1779–83
[34] Batra R C and Geng T S 2002 Comparison of active constrained layer damping by using extension and shear mode actuators *J. Intell. Mater. Syst. Struct.* **13** 249–367
[35] Batra R C and Vidoli S 2002 Higher order piezoelectric plate theory derived from a three-dimensional variational principle *AIAA J.* **40** 91–104
[36] Batra R C, Vidoli S and Vestroni F 2002 Plane waves and modal analysis in higher-order shear and normal deformable plate theories *J. Sound Vib.* **257** 63–8